Electronic Supplementary Material (ESI) for Inorganic Chemistry Frontiers.
This journal is © the Partner Organisations 2024

**Supporting Information**

# Continuous Regulating Cu Electronic States by Rectifying Schottky Contacts Enhancing Electrochemical Nitrate Reduction to Ammonia

Yuzhuo Zhou, Wenlin Zhang*, Peng Guo, Yabo Guo, Jiayu Zhan, Yaheng Wang, Bo Zhang, Shaobo Zhang, Lu-Hua Zhang and Fengshou Yu*

National-Local Joint Engineering Laboratory for Energy Conservation in Chemical Process Integration and Resources Utilization, School of Chemical Engineering and Technology, Hebei University of Technology, Tianjin 300130, P. R. China.

E-mail: yfsh@hebut.edu.cn; ctstzwl@163.com

## Chemicals and Materials

### Chemicals.

Copper(II) acetate monohydrate ($C_4H_6CuO_4 \cdot H_2O$, AR 99%), L-Glutamic acid ($C_5H_9NO_4$, 99%), 1,3,5-Benzenetricarboxylic acid ($C_9H_6O_6$, 98%), hexadecyl trimethyl ammonium bromide ($C_{19}H_{42}BrN$, 98%) were obtained from Aldrich. Dicyandiamide ($C_2H_4N_4$, 99.8%) was purchaseed from the Sinopharm Chemical Reagent Co. All chemicals were used as supplied without further purification.

### Synthesis of precursor.

Firstly, Copper(II) acetate monohydrate (0.836 g) and L-glutamic acid (0.308 g) were soluted in DI water (200 mL). Then dissolved 1,3,5-benzenetricarboxylic acid (0.464 g) and hexadecyl trimethyl ammonium bromide (0.124 g) into the mixture of DI water (180 mL) and ethanol (20 mL), then added to the aforementioned liquid at moderate stirring. After stirring for 2 h at room temperature, the solid material was rinsed three times by centrifugation with DI water and collected as a light blue solid material, which was dried under vacuum at 60 °C overnight.

### Synthesis of Cu@$N_x$C.

The precursor (0.4 g) was blended with dicyandiamide (1.0 g) and ground well in a agate mortar. Afterwards, the mixed solid was placed in an aluminium crucible and heated at 700 ℃ for 3 h under Ar with a crawling speed of 3 ℃ $min^{-1}$. Cu@$N_{0.2}$C, Cu@$N_{0.5}$C, Cu@$N_{1.0}$C and Cu@$N_{2.0}$C were fabricated by adjusting the quantity of dicyandiamide to 0.2 g, 0.5 g, 1 g and 2g, respectively.

### Synthesis of Cu@C.

Cu@C was synthesized by a similar process with Cu@$N_x$C in the absence of dicyandiamide.

### Synthesis of NC.

NC was synthesized by a similar process without addition of $Cu(CO_2CH_3)_2 \cdot H_2O$.

### Characterization.

SEM images were obtained on a Tescan MIRA LMS and TEM images were acquired on an FEI Talos F200XG2 AEMC. XRD patterns were collected on a Rigaku Ultima IV microscope. XPS spectroscopy was carried out on a Thermo Scientific K-Alpha. ICP-MS was derived by Aglient 7800 (MS). UV-vis detection of

ion concentrations was accomplished using a TU-1900. Isotope labeling experiments were performed using $^1$H NMR on BRUKER AVANCE 400.

**Electrochemical measurements.**

The electrochemical measurements were conducted with a prototype three-electrode H-type cell using an electrochemical workstation (CHI760E). To fabricate the working electrode, 4.0 mg of sample and 50 μL of Nafion (5 wt.%) were dispersed in a blend of 475 μL ethanol and 475 μL ultrapure water and then ultrasonicated for approximately 30 min to form a homogeneous solution. Afterwards, the electrocatalyst ink was spread on the carbon paper in a smooth layer to attain a loading of 0.2 mg cm$^{-2}$ as working electrode.

**The calculation method of $FE_{NH_3}$**

The Faraday efficiency of the $NH_3$ product is calculated as follows.

$$FE_{NH_3} = \left(8 \times F \times C_{NH_3} \times V\right)/(M_{NH_3} \times Q)$$

$C_{NH_3}$: Measured $NH_4^+$ concentration (mg L$^{-1}$).

V: Volume of electrolyte (mL).

F: Faraday standard value (96485 C mol$^{-1}$).

Q: Gross electric charge (C).

**The calculation method of $NH_3$ yield**

The yield of $NH_3$ product is calculated as follows.

$$Yield\ NH_3 = \left(C_{NH_3} \times V\right)/(M_{NH_3} \times t \times m)$$

$C_{NH_3}$: Measured $NH_4^+$ concentration (mg L$^{-1}$).

V: Capacity of electrolyte (mL).

$M_{NH_3}$: Specific relative molecular mass of ammonia.

t: Electrolysis time.

m: The mass of catalyst.

**Isotopic labeling experiment**

The electrochemical investigations presented in the above sections were performed in the $NO_3$RR isotopic

labelling experiments employing $Na^{15}NO_3$ as the N source. Afterwards, 500 μL of the electrolyte was combined with 200 μL of $d^6$-DMSO for the $^1H$ NMR experiment.

**Simulation calculations**

The Vienna Ab initio Simulation Package (VASP) was applied for the density functional theory (DFT) calculations in this study. The projector augmented wave (PAW) method was performed with the Perdew-Burke-Ernzerhof (PBE) generalized gradient approximation (GGA) exchange-correlation energy. As revealed by the X-ray diffraction pattern, the primary crystal plane of the metal Cu is the (111) crystal plane, so the Cu (111) crystal plane is adopted as the most stable model incorporating the [3×3] supercell structures. The Cu@C model was established by combining the carbon substrate (C) on the nanometric surface of Cu, and the $Cu@N_{1.0}C$ model was constructed by embedding N atom on carbon substrate. The Cu(111) surface is presented as an extremely robust cuboctahedral geometry with two-dimensional regular boundary conditions. To prevent interference with neighbouring layers, we set a vacuum of 15 Å according to the z-axis direction. The electronic structure and geometry convergence criteria are specified at $1.0\times10^{-5}$ eV and -0.02 eV/Å, respectively. The threshold energy is adjusted to 400 eV.

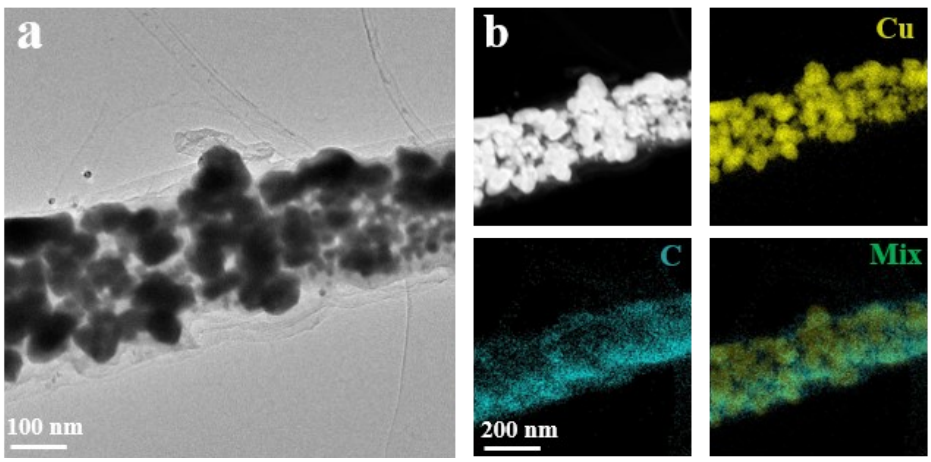


**Figure S1.** (a) TEM and (b) EDS elemental mappings images of Cu@C.

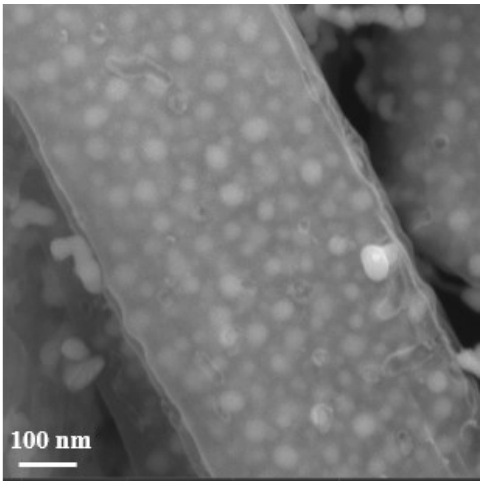


**Figure S2.** SEM image of $Cu@N_{1.0}C$.

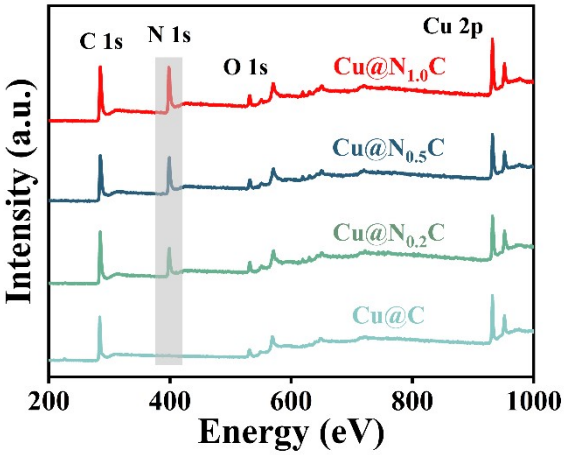


**Figure S3.** XPS spectra of $Cu@N_{1.0}C$, $Cu@N_{0.5}C$, $Cu@N_{0.2}C$ and Cu@C.

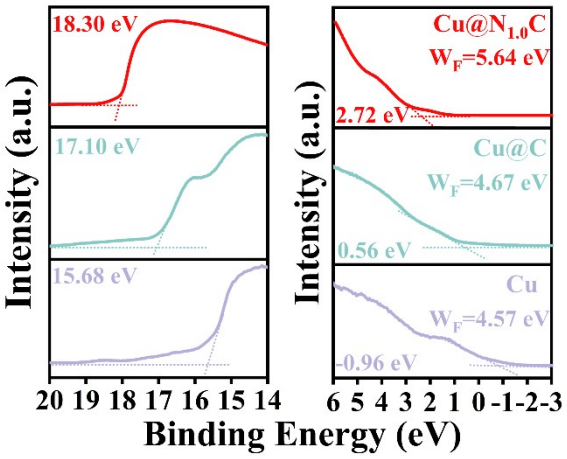


**Figure S4.** UPS spectra of $Cu@N_{1.0}C$, Cu@C and Cu.

The Cu@C sample presents a lower work function of 4.67 eV than that for $Cu@N_{1.0}C$ (5.64 eV), indicating that more electrons were transferred to NC due to doping with N.

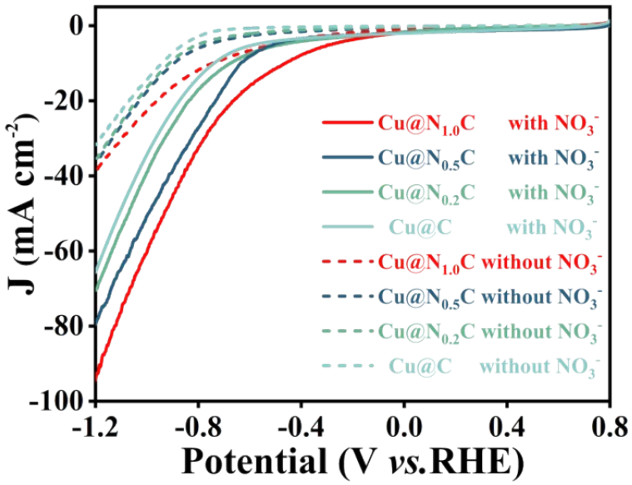


**Figure S5.** LSV curves of $Cu@N_{1.0}C$, $Cu@N_{0.5}C$, $Cu@N_{0.2}C$ and Cu@C in 0.5 M $Na_2SO_4$ (PH=11.5) with or without $NO_3^-$.

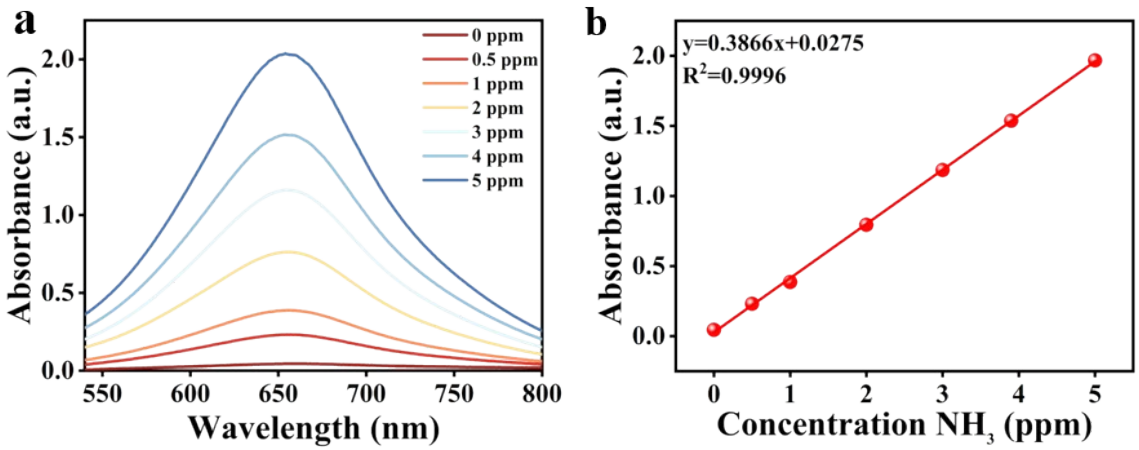


**Figure S6.** (a) Ultraviolet absorption and (b) concentration-absorbance calibration curves of $NH_4^+$.

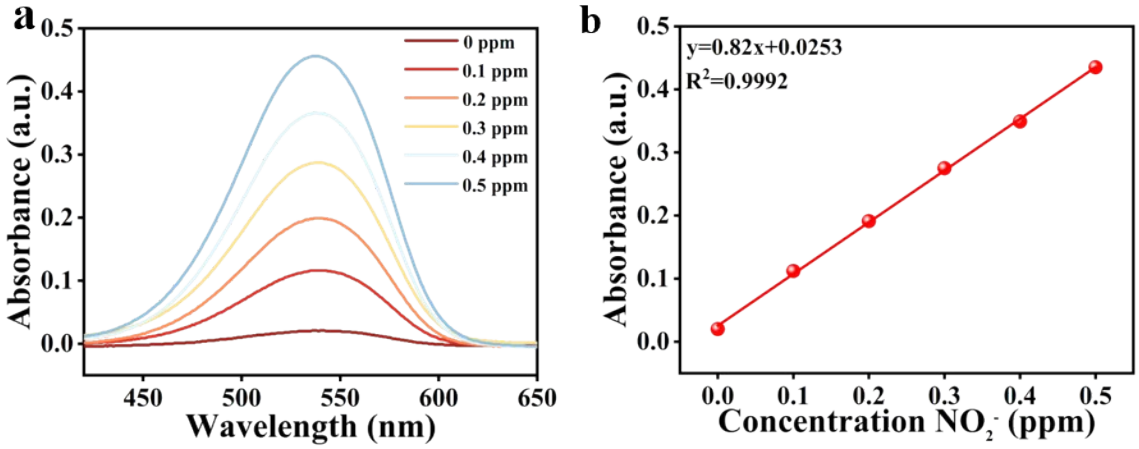


**Figure S7**. (a) Ultraviolet absorption and (b) concentration-absorbance calibration curves of $NO_2^-$.

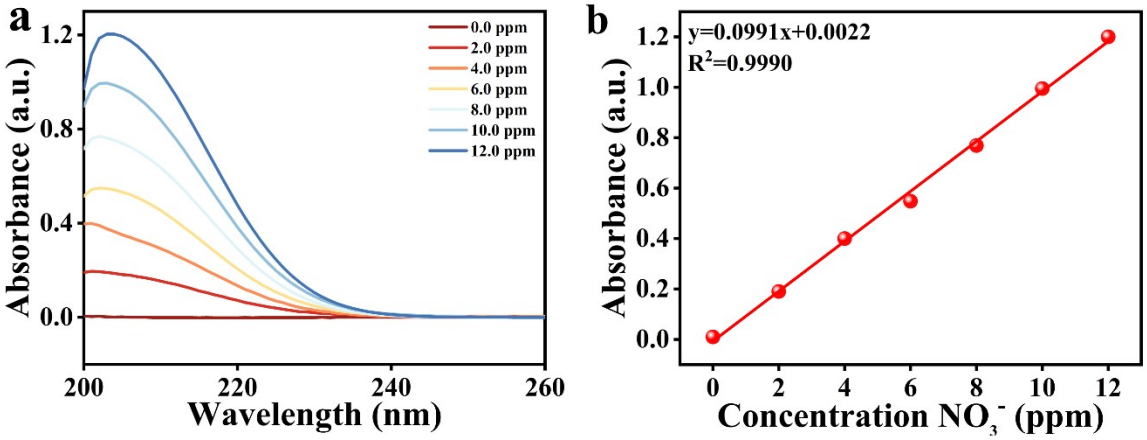


**Figure S8**. (a) Ultraviolet absorption and (b) concentration-absorbance calibration curves of $NO_3^-$.

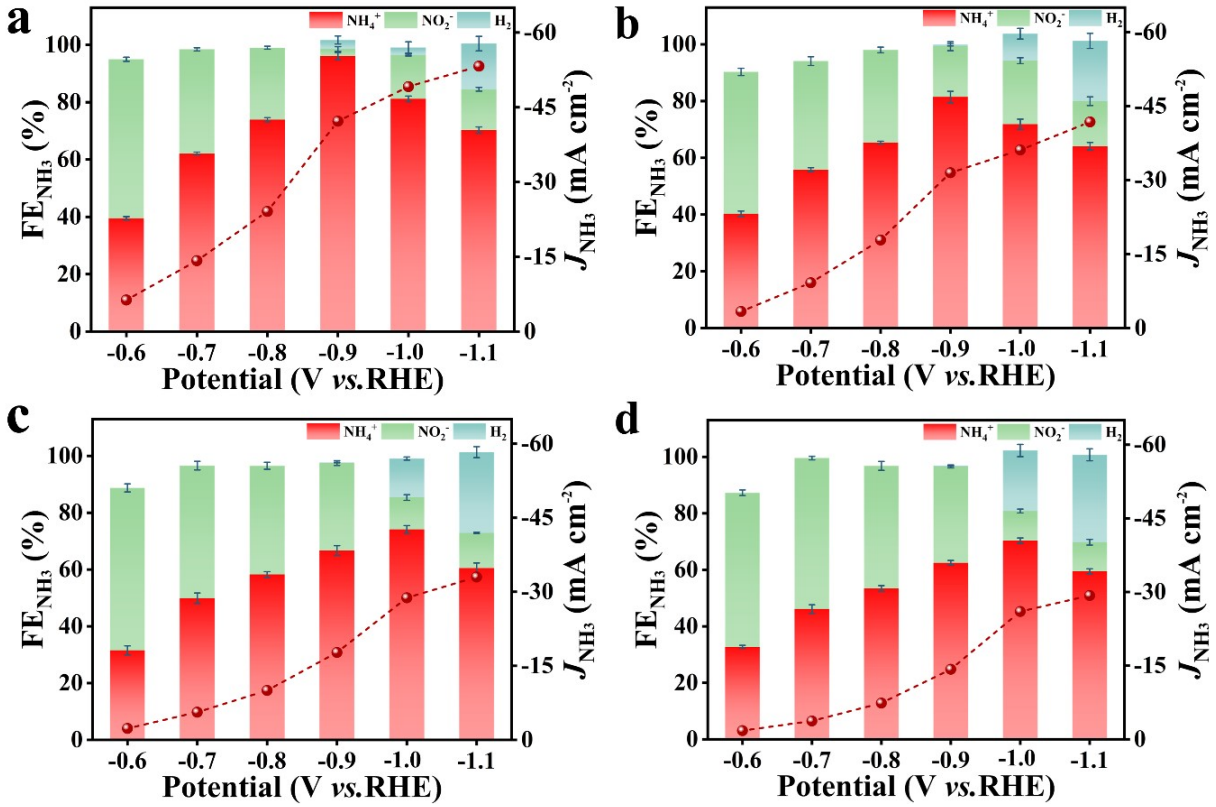


**Figure S9.** FE of $NH_3$, $H_2$ and $NO_2^-$ productions with (a) $Cu@N_{1.0}C$, (b) $Cu@N_{0.5}C$, (c) $Cu@N_{0.2}C$ and (d) Cu@C.

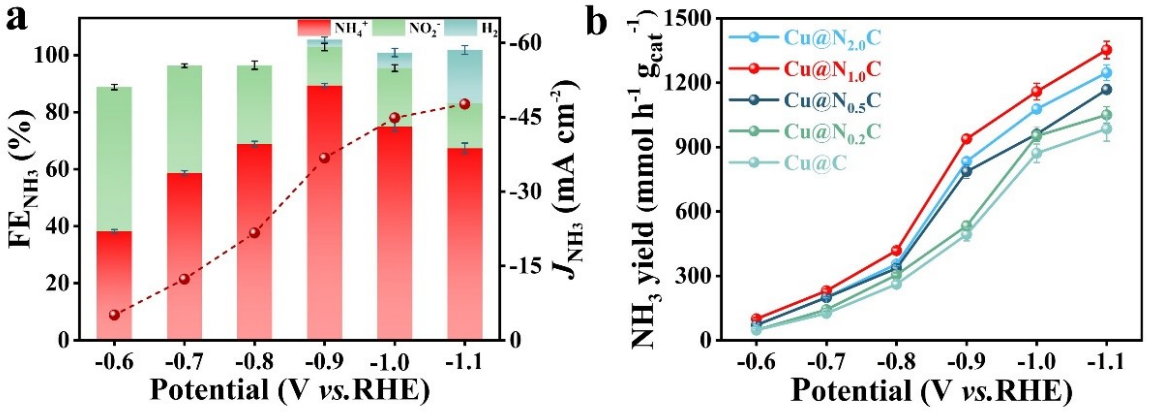


**Figure S10.** (a) FE of $NH_3$, $H_2$ and $NO_2^-$ productions with $Cu@N_{2.0}C$; (b) Yield rate of $NH_3$ of each catalyst.

The doping amount of dicyandiamide was further increased to fabricate sample Cu@$N_{2.0}$C. The results showed that the elevated doping of dicyandiamide did not increase the $NH_3$ Faraday efficiency, current density and yield of Cu@$N_{2.0}$C, This is consistent with previous XPS analyses that further enhancement of dicyandiamide doping did not correspondingly increase its N content.

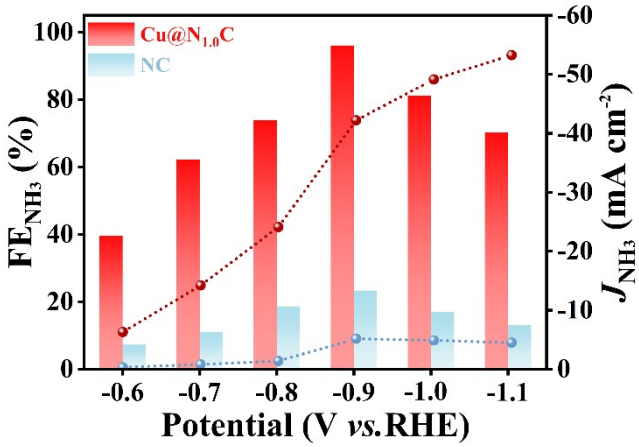


**Figure S11.** FE of $NH_3$ of Cu@$N_{1.0}$C and NC at various potentials.

The NC samples exhibit extremely low $NH_3$ Faraday efficiencies and current densities compared to Cu@$N_{1.0}$C sample. This means the excellent $NO_3$RR performance is achieved after Cu nanoparticle loaded, therefore the active site is on Cu.

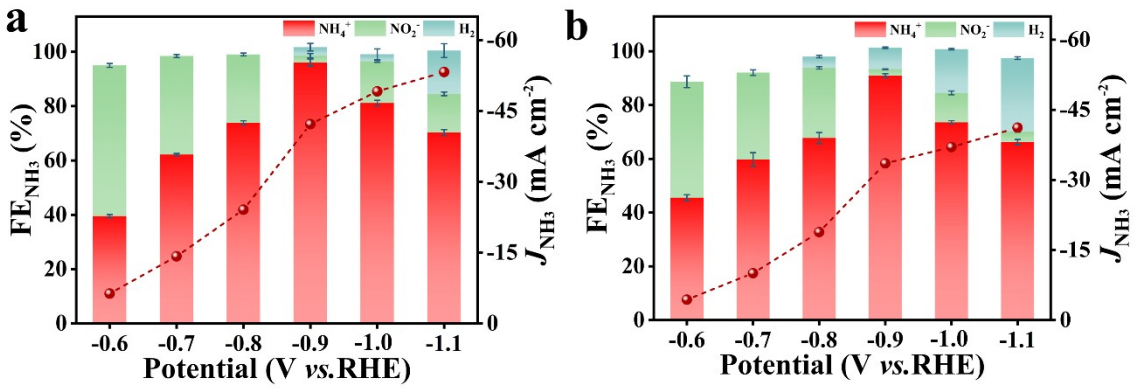


**Figure S12.** FE of $NH_3$, $H_2$ and $NO_2^-$ productions with Cu@$N_{1.0}$C in (a) 0.5 M $Na_2SO_4$ (pH=11.5) and (b) 0.5 M PBS with 0.1 M $NaNO_3$.

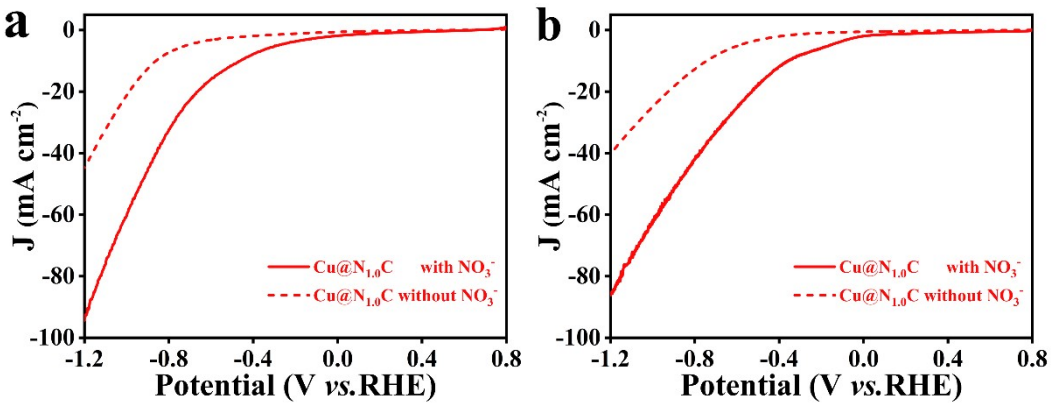


**Figure S13.** LSV curves of Cu@$N_{1.0}$C in (a) 0.5 M $Na_2SO_4$ (pH=11.5) and (b) 0.5 M $K_2SO_4$ (pH=11.5) with or without 0.1 M $NaNO_3$.

The $K_2SO_4$ is employed instead of $Na_2SO_4$ to investigate the ions acting in the electrolyte. The results showed that catalytic current density was not significantly changed compared to $Na_2SO_4$, confirming that $SO_4^{2-}$ has a more important role in enhancing electrical conductivity.

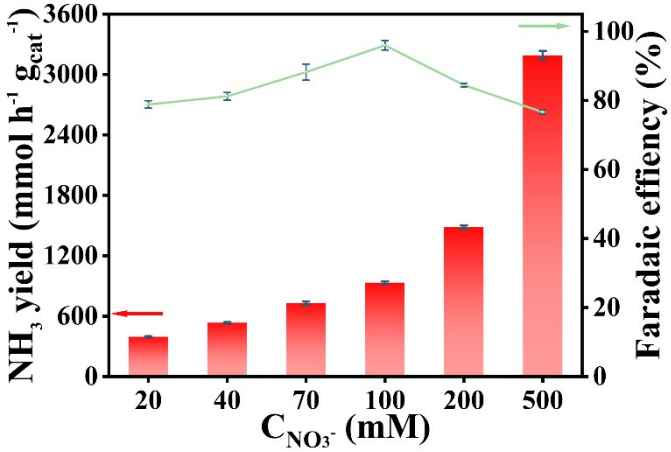


**Figure S14.** The $NH_3$ yield and selectivity of Cu@$N_{1.0}$C with $NO_3^-$ concentrations ranging from 20 to 500 mM.

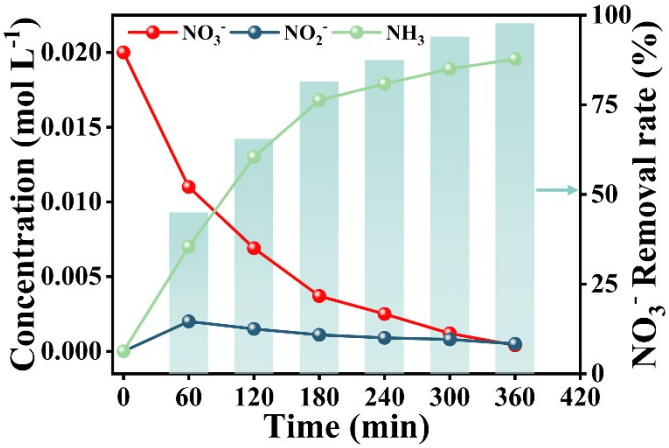


**Figure S15.** Time-dependent concentration changes of $NO_3^-$, $NH_3$, and $NO_2^-$ by Cu@$N_{1.0}$C at -0.9 V. After 6

h of electrolysis, the removal rate of $NO_3^-$ reached 97.8%.

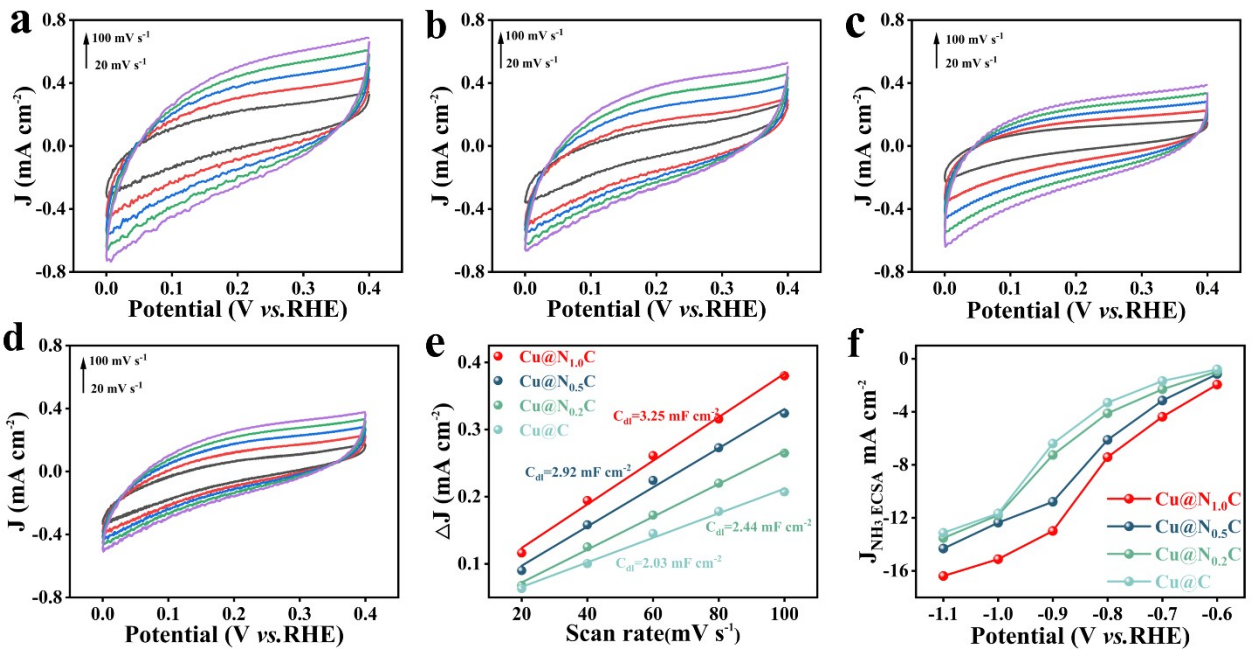


**Figure S16.** CV curves at various scan rates of (a) Cu@$N_{1.0}$C, (b) Cu@$N_{0.5}$C, (c) Cu@$N_{0.2}$C and (d) Cu@C; (e) the corresponding $C_{dl}$ by ECSA; (f) the ECSA normalized current density for $NH_3$ formation.

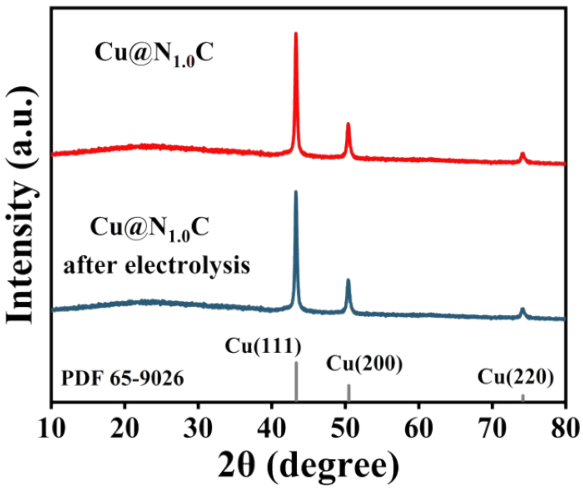


**Figure S17.** (a) XRD patterns of Cu@$N_{1.0}$C before and after electrolysis at -0.9 V.

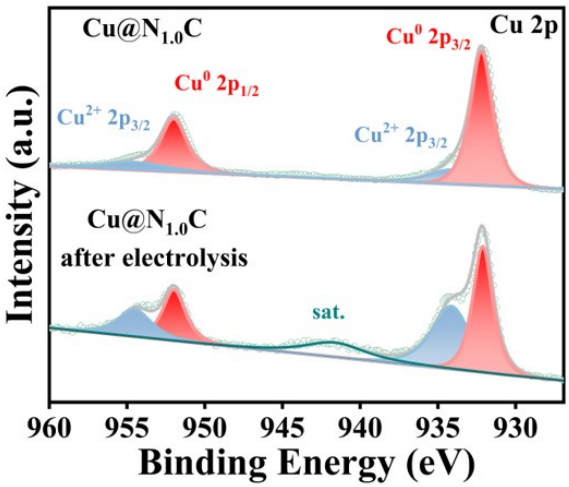


**Figure S18.** (a) XPS spectra of $Cu@N_{1.0}C$ before and after electrolysis at -0.9 V.

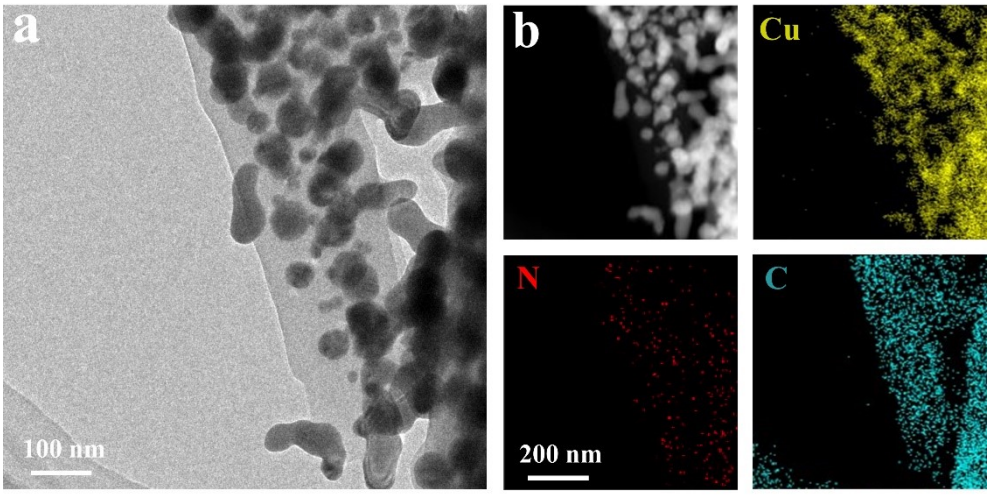


**Figure S19.** (a) TEM and (b) EDS elemental mapping images of $Cu@N_{1.0}C$ after electrolysis at -0.9V.

**Table S1.** Element contents of Cu@$N_{2.0}$C, Cu@$N_{1.0}$C, Cu@$N_{0.5}$C, Cu@$N_{0.2}$C, Cu@C and NC samples estimated from XPS analysis.

| Sample | Cu (at. %) | N (at. %) | C (at. %) |
|---|---|---|---|
| NC | 0 | 15.78 | 84.22 |
| Cu@C | 7.48 | 0 | 92.52 |
| Cu@$N_{0.2}$C | 6.99 | 6.32 | 86.69 |
| Cu@$N_{0.5}$C | 6.73 | 10.18 | 83.09 |
| Cu@$N_{1.0}$C | 6.87 | 16.12 | 77.01 |
| Cu@$N_{2.0}$C | 7.06 | 14.78 | 78.16 |

The N contents of Cu@$N_x$C samples can be tuned with adding different amounts of dicyanodiamine (DCD) as additional N source, and the highest N content can reach 16.12 at.%. When more DCD was used, the N content never continues to increase. Therefore, the N content for this work was at the range of 0-16.12 at.%.

**Table S2.** The contents of Cu in Cu@$N_{1.0}$C, Cu@$N_{0.5}$C, Cu@$N_{0.2}$C and Cu@C determined by ICP-MS.

| Sample | Cu (wt. %) |
|---|---|
| Cu@$N_{1.0}$C | 39.92 |
| Cu@$N_{0.5}$C | 40.63 |
| Cu@$N_{0.2}$C | 42.11 |
| Cu@C | 43.45 |

**Table S3.** Different N contents from N1s spectra of Cu@$N_{1.0}$C, Cu@$N_{0.5}$C, Cu@$N_{0.2}$C and NC.

| Sample | Pyridine N (at. %) | Pyrrolic N (at. %) | Graphitic N (at. %) |
|---|---|---|---|
| Cu@$N_{1.0}$C | 72.12 | 14.91 | 12.97 |
| Cu@$N_{0.5}$C | 69.55 | 15.54 | 14.91 |
| Cu@$N_{0.2}$C | 69.00 | 16.91 | 14.09 |
| NC | 55.26 | 31.04 | 13.70 |

**Table S4.** Comparison of $NH_3$ selectivity and yield rate by $NO_3RR$ on various catalysts.

| Catalysts | Electrolyte | $FE_{NH_3}$(%) | Potential (vs. RHE) | $NH_3$ yield rate (mmol $h^{-1}$ $g_{cat}^{-1}$) | Ref. |
|---|---|---|---|---|---|
| $NiO_4$-CCP | 0.5 M $NO_3^-$<br>1 M $Na_2SO_4$ | 94.7 | -0.7 | 1830.0 | [1] |
| np-Cu/$MnO_x$ | 0.1 M $NaNO_3$<br>0.1 M $Na_2SO_4$ | 86.2 | -0.75 | 1723.5 | [2] |
| **Cu@$N_{1.0}$C** | **0.1 M $NaNO_3$**<br>**0.5 M $Na_2SO_4$**<br>**（pH=11.5）** | **96.2**<br><br>**71.43** | **-0.9**<br><br>**-1.1** | **934.8**<br><br>**1353.1** | **This work** |
| $Ag_{30}Pd_4$ | 1500 ppm $NO_3^-$-N<br>1 M KOH | 90.1 | -0.6 | 1280.0 | [3] |
| Pd@FeNi-CoO | 500 ppm $KNO_3$<br>0.5 M $K_2SO_4$ | 100.0 | -0.8 | 1191.8 | [4] |
| Fe SAC | 0.5 M $KNO_3$<br>0.1 M $K_2SO_4$ | 75.0 | -0.85 | 1176.5 | [5] |
| Fe/Cu-NG | 0.1 M $KNO_3$<br>1 M KOH | 92.51 | -0.5 | 1080 | [6] |
| $Fe_2TiO_5$ | 0.1 M $NaNO_3$<br>PBS | 87.5 | -1.0 | 772.4 | [7] |
| Cu-N-C | 0.1 M $KNO_3$<br>0.1 M KOH | 84.7 | -1.0 | 735.3 | [8] |
| BCN@Cu | 0.1 M $KNO_3$<br>0.1 M KOH | 88.9 | -0.6 | 576.2 | [9] |
| CuO@$CuFe_2O_4$ | 0.1 M $NaNO_3$<br>0.1 M PBS | 91.08 | -1.0 | 541.8 | [10] |
| Pd-NDs/Zr-MOF | 0.05 M $NaNO_3$<br>0.1 M $Na_2SO_4$ | 58.1 | -1.3 | 287.3 | [11] |
| RC-SnK-800 | 0.1 M $NaNO_3$<br>0.5 M $Na_2SO_4$ | 93.4 | -0.99 | 221.1 | [12] |
| Au-NCs/PtTeAu-MLs | 0.05 M $KNO_3$<br>0.5 M $H_2SO_4$ | 96.3 | -0.03 | 205.8 | [13] |
| PA-RhCu cNCs | 0.05 M $NaNO_3$<br>0.1 M $HClO_4$ | 93.7 | 0.05 | 141.2 | [14] |
| Fe/$Ni_2P$ | 0.05 M NaNO2<br>0.2 M $K_2SO_4$ | 100.0 | -0.4 | 122.4 | [15] |

**Table S5.** Comparison of selectivity and yield rate by $NO_3RR$ on various catalysts (Standardized per gram of Cu).

| Catalysts | Electrolyte | $FE_{NH_3}$(%) | Potential (vs. RHE) | $NH_3$ yield rate (mmol $h^{-1}$ $gCu^{-1}$) | Ref. |
|---|---|---|---|---|---|
| Zn/Cu-2.3 | 0.1 M $KNO_3$<br>0.5 M $K_2SO_4$ | 98.4 | -0.55 | 5918.4 | [16] |
| **$Cu@N_{1.0}C$** | **0.1 M $NaNO_3$**<br>**0.5 M $Na_2SO_4$**<br>**（pH=11.5）** | **96.2**<br><br>**71.43** | **-0.9**<br><br>**-1.1** | **2341.7**<br><br>**3389.5** | **This work** |
| $Cu_{0.25}Ni_{0.25}$ | 0.75 M $KNO_3$<br>1 M KOH | 94.5 | -0.3 | 2610.7 | [17] |
| $Cu_{50}Co_{50}$ | 0.1 M $KNO_3$<br>1 M KOH | 100.0 | -0.2 | 1882.4 | [18] |
| Cu@NHC | 0.1 M $NaNO_3$<br>0.1 M $Na_2SO_4$ | 77.1 | -0.8 | 1880.4 | [19] |
| np Ru-Cu | 0.05 M $KNO_3$<br>0.1 M KOH | 97.3 | -0.2 | 1796.8 | [20] |
| CuCo/NC | 0.2 M $NaNO_3$<br>0.5 M $Na_2SO_4$ | 95.1 | -0.79 | 561.1 | [21] |
| Cu@C | 0.001 M $NO_3^-$ | 72.0 | -0.3 | 57.9 | [22] |
| Cu nanosheets | 0.01 M $KNO_3$<br>0.1 M KOH | 99.7 | -0.15 | 22.9 | [23] |

Comparison of the $NH_3$ yield and Faraday efficiency of the catalysts on a per gram of Cu basis, taking into account the metal utilization of the Cu-based materials. The results show that $Cu@N_{1.0}C$ can achieve higher performance. This suggests that metal costs can be significantly reduced when substantial amounts of $NH_3$ are produced, which offers greater promise for future practical applications.

**Table S6.** The content of Cu in $Cu@N_{1.0}C$ determined by ICP-MS before and after 20 times testing.

| Sample | Electrolytic state | Cu (wt. %) |
|---|---|---|
| $Cu@N_{1.0}C$ | Before | 39.92 |
| | After | 38.78 |

**Table S7.** Element contents of Cu@$N_{1.0}$C sample estimated from XPS analysis before and after 20 times testing.

| Sample | Cu (at. %) | N (at. %) | C (at. %) |
|---|---|---|---|
| Before | 6.87 | 16.12 | 77.01 |
| After | 6.63 | 15.88 | 77.49 |

REFERENCES


1 Y. Zhang, H. Zheng, K. Zhou, J. Ye, K. Chu, Z. Zhou, L. Zhang and T. Liu, Conjugated Coordination Polymer as a New Platform for Efficient and Selective Electroreduction of Nitrate into Ammonia, *Adv. Mater*., 2023, **35**, 2209855.

2 Y. Cui, A. Dong, Y. Zhou, Y. Qu, M. Zhao, Z. Wang and Q. Jiang, Interfacially Engineered Nanoporous Cu/$MnO_x$ Hybrids for Highly Efficient Electrochemical Ammonia Synthesis via Nitrate Reduction, *Small*, 2023, **19**, 2207661.

3 L. Qin, F. Sun, Z. Gong, G. Ma, Y. Chen, Q. Tang, L. Qiao, R. Wang, Z.-Q. Liu and Z. Tang, Electrochemical $NO_3^-$ Reduction Catalyzed by Atomically Precise $Ag_{30}Pd_4$ Bimetallic Nanocluster: Synergistic Catalysis or Tandem Catalysis? *ACS Nano*, 2023, **17**, 12747-12758.

4 H. Fu, Y. Chen, H. Huang, C. Chen, T. Zhu, F. Lai, N. Zhang and T. Liu, Enhanced Metal−Support Interfacial Interaction of Pd@FeNi-CoO Composites for Efficient Nitrate Reduction to Ammonia, *ACS Sustain. Chem. Eng.*, 2023, 12, 346-354.

5 Z.-Y. Wu, M. Karamad, X. Yong, Q. Huang, D. A. Cullen, P. Zhu, C. Xia, Q. Xiao, M. Shakouri, F.-Y. Chen, J. Y. Kim, Y. Xia, K. Heck, Y. Hu, M. S. Wong, Q. Li, I. Gates, S. Siahrostami and H. Wang, Electrochemical ammonia synthesis via nitrate reduction on Fe single atom catalyst, *Nat. Commun*., 2021, **12**, 2870.

6 S. Zhang, J. Wu, M. Zheng, X. Jin, Z. Shen, Z. Li, Y. Wang, Q. Wang, X. Wang, H. Wei, J. Zhang, P. Wang, S. Zhang, L. Yu, L. Dong, Q. Zhu, H. Zhang and J. Lu, Fe/Cu diatomic catalysts for electrochemical nitrate reduction to ammonia, *Nat. Commun*., 2023, **14**, 3634.

7 H. Du, H. Guo, K. Wang, X. Du, B. A. Beshiwork, S. Sun, Y. Luo, Q. Liu, T. Li and X. Sun, Durable Electrocatalytic Reduction of Nitrate to Ammonia over Defective Pseudobrookite $Fe_2TiO_5$ Nanofibers with Abundant Oxygen Vacancies, *Angew. Chem. Int. Ed*., 2022, **62**, e202215782.

8 J. Yang, H. Qi, A. Li, X. Liu, X. Yang, S. Zhang, Q. Zhao, Q. Jiang, Y. Su, L. Zhang, J.-F. Li, Z.-Q. Tian, W. Liu, A. Wang and T. Zhang, Potential-Driven Restructuring of Cu Single Atoms to Nanoparticles for Boosting the Electrochemical Reduction of Nitrate to Ammonia, *J. Am. Chem. Soc.*, 2022, **144**, 12062-12071.

9 X. Zhao, G. Hu, F. Tan, S. Zhang, X. Wang, X. Hu, A. V. Kuklin, G. V. Baryshnikov, H. Ågren, X. Zhou and H. Zhang, Copper confined in vesicle-like BCN cavities promotes electrochemical reduction of nitrate to ammonia in water, *J. Mater. Chem A*, 2021, **9**, 23675-23686.

10 H. Zhu, S. Dong, X. Du, H. Du, J. Xia, Q. Liu, Y. Luo, H. Guo and T. Li, Defective CuO-rich $CuFe_2O_4$ nanofibers enable the efficient synergistic electrochemical reduction of nitrate to ammonia, *Catal. Sci. Technol*., 2022, **12**, 4998-5002.

11 M. Jiang, J. Su, X. Song, P. Zhang, M. Zhu, L. Qin, Z. Tie, J.-L. Zuo and Z. Jin, Interfacial Reduction Nucleation of Noble Metal Nanodots on Redox-Active Metal−Organic Frameworks for High-Efficiency Electrocatalytic Conversion of Nitrate to Ammonia, *Nano Letter.*, 2022, **22**, 2529-2537.
12 X. Zheng, Z. Tian, R. Bouchal, M. Antonietti, N. López-Salas and M. Odziomek, Tin (II) Chloride Salt Melts as Non-Innocent Solvents for the Synthesis of Low-Temperature Nanoporous Oxo-Carbons for Nitrate Electrochemical Hydrogenation, *Adv. Mater.*, 2023, 2311575.
13 Q. L. Hong, B. Sun, X. Ai, X. L. Tian, F. M. Li and Y. Chen, Au Nanocrystals Modified Holey PtTeAu Metallene Heteronanostructures for Plasmon-Enhanced Nitrate Electroreduction, *Adv. Funct. Mater.*, 2023, 2310730.
14 Z. X. Ge, T. J. Wang, Y. Ding, S. B. Yin, F. M. Li, P. Chen and Y. Chen, Interfacial Engineering Enhances the Electroactivity of Frame-Like Concave RhCu Bimetallic Nanocubes for Nitrate Reduction, *Adv. Energy Mater.*, 2022, **12**, 2103916.
15 R. Zhang, Y. Guo, S. Zhang, D. Chen, Y. Zhao, Z. Huang, L. Ma, P. Li, Q. Yang, G. Liang and C. Zhi, Efficient Ammonia Electrosynthesis and Energy Conversion through a Zn-Nitrate Battery by Iron Doping Engineered Nickel Phosphide Catalyst, *Adv. Energy Mater.*, 2022, **12**, 2103872.
16 L. Wu, J. Feng, L. Zhang, S. Jia, X. Song, Q. Zhu, X. Kang, X. Xing, X. Sun and B. Han, Boosting Electrocatalytic Nitrate-to-Ammonia via Tuning of N-Intermediate Adsorption on a Zn−Cu Catalyst, Angew. Chem. Int. Ed., 2023, 62, e202307952.
17 J. Wang, L. Zhang, Y. Wang, Y. Niu, D. Fang, Q. Su and C. Wang, Facet and d-band center engineering of CuNi nanocrystals for efficient nitrate electroreduction to ammonia, Dalton Trans., 2022, 51, 15111-15120.
18 J.-Y. Fang, Q.-Z. Zheng, Y.-Y. Lou, K.-M. Zhao, S.-N. Hu, G. Li, O. Akdim, X.-Y. Huang and S.-G. Sun, Ampere-level current density ammonia electrochemical synthesis using CuCo nanosheets simulating nitrite reductase bifunctional nature, Nat. Commun., 2022, 13, 7899.
19 J. Zhang, C. Chen, R. Zhang, X. Wang, Y. Wei, M. Sun, Z. Liu, R. Ge, M. Ma and J. Tian, Size-induced d band center upshift of copper for efficient nitrate reduction to ammonia, J. Colloid Interface Sci., 2024, 658, 934-942.
20 Y. Cui, C. Sun, G. Ding, M. Zhao, X. Ge, W. Zhang, Y. Zhu, Z. Wang and Q. Jiang, Synergistically tuning intermediate adsorption and promoting water dissociation to facilitate electrocatalytic nitrate reduction to ammonia over nanoporous Ru-doped Cu catalyst, Sci. China Mater., 2023, 66, 4387-4395.
21 J. Cheng, G. Dai, W. Sun, X. Yang, R. Xia, Y. Xu and Y. Mao, Carbon Nanocage Confining CuCo Bimetallic Interface with Low Nitrate Adsorption Energy for Highly Efficient Electrochemical Ammonia Synthesis, Energy Fuels, 2024, 38, 2501-2510.
22 Z. Song, Y. Liu, Y. Zhong, Q. Guo, J. Zeng and Z. Geng, Efficient Electroreduction of Nitrate into Ammonia at Ultralow Concentrations Via an Enrichment Effect, Adv. Mater., 2022, 34, 2204306.
23 X. Fu, X. Zhao, X. Hu, K. He, Y. Yu, T. Li, Q. Tu, X. Qian, Q. Yue, M. R. Wasielewski and Y. Kang, Alternative route for electrochemical ammonia synthesis by reduction of nitrate on copper nanosheets, Appl. Mater. Today, 2020, 19, 100620.